

## THE BANANA PROJECT. IV. TWO ALIGNED STELLAR ROTATION AXES IN THE YOUNG ECCENTRIC BINARY SYSTEM EP CRUCIS: PRIMORDIAL ORIENTATION AND TIDAL ALIGNMENT\*

SIMON ALBRECHT<sup>1</sup>, JOHNY SETIAWAN<sup>2,3</sup>, GUILLERMO TORRES<sup>4</sup>, DANIEL C. FABRYCKY<sup>5</sup>, JOSHUA N. WINN<sup>1</sup>,  
*Draft version October 27, 2018*

### ABSTRACT

With observations of the EP Cru system, we continue our series of measurements of spin-orbit angles in eclipsing binary star systems, the BANANA project (Binaries Are Not Always Neatly Aligned). We find a close alignment between the sky projections of the rotational and orbital angular momentum vectors for both stars ( $\beta_p = -1.8 \pm 1.6^\circ$  and  $|\beta_s| < 17^\circ$ ). We also derive precise absolute dimensions and stellar ages for this system. The EP Cru and DI Her systems provide an interesting comparison: they have similar stellar types and orbital properties, but DI Her is younger and has major spin-orbit misalignments, raising the question of whether EP Cru also had a large misalignment at an earlier phase of evolution. We show that tidal dissipation is an unlikely explanation for the good alignment observed today, because realignment happens on the same timescale as spin-orbit synchronization, and the stars in EP Cru are far from synchronization (they are spinning 9 times too quickly). Therefore it seems that some binaries form with aligned axes, while other superficially similar binaries are formed with misaligned axes.

*Subject headings:* stars: kinematics and dynamics – stars: early-type – stars: rotation – stars: formation – binaries: eclipsing – stars: individual (EP Crucis) – stars: individual (DI Herculis) – techniques: spectroscopic

### 1. INTRODUCTION

One might expect star-planet and close binary star systems to have well-aligned orbital and rotational angular momenta, since they originate from the same portion of a molecular cloud. However, there are also reasons to expect misaligned systems. Star formation is a chaotic process, with accretion from different directions at different times possibly leading to misalignment between the stellar and orbit rotation axes (e.g., Bate et al. 2010; Thies et al. 2011). There are also processes that could alter the stellar and orbital spin directions after their formation. For example a third body orbiting a close pair on a highly inclined orbit can introduce large oscillations in the orbital inclination and eccentricity of the close pair (Kozai 1962), thereby introducing large angles between the stellar spins and orbital angular momentum of the close pair. Close encounters and possible exchange of members in binary systems (e.g., Gualandris et al. 2004) would leave, among other clues, a fingerprint in the form of misalignment between the components. Tidal forces will over time erase these clues, because dissipation will tend to bring the axes into alignment while also synchronizing the rotational and orbital periods (e.g., Zahn 1977; Hut 1981; Eggleton & Kiseleva-Eggleton 2001). Thus the degree of alignment between the stellar rotation axes and the orbital axis depends on its particular history of formation and evolution. Therefore measurements of stel-

lar obliquities – the angle between stellar equator and orbital plane – allow us to test theories of formation and evolution in close star-planet and star-star systems.

For example the formation of star-star systems with orbital distances of only a few stellar radii is not completely understood. It seems unlikely that the stars formed at these orbital distances because they would have overlapped during their pre-main sequence phase, when they had larger sizes. Therefore the orbital distance likely decreased after formation. A possible mechanism is KCTF – Kozai Cycles with Tidal Friction (Eggleton & Kiseleva-Eggleton 2001; Fabrycky & Tremaine 2007), which requires a third body on a wide orbit around the close pair. Tokovinin et al. (2006) found that 96% of binary stars with orbital periods less than 3 days have a third companion on a wide orbit while only 34% of binaries with orbital periods larger than 12 days have a third companion. Additional evidence for KCTF would be a misalignment between the stellar spin axes and the orbital spin, assuming that close binaries have aligned axes at birth, and that tides have not had enough time to align the spin axes. Thus measurements of stellar obliquities in close binary systems together with a good understanding of tidal dissipation in these systems might lead to a better understanding of binary formation.

For the case of close star-planet (hot-Jupiter) systems such an approach has been fruitful. Hot-Jupiters are thought to have formed much further from the star than their current orbital distances, mainly because not enough material would have been available so close to the star. Different processes which could have transported the planet inward would lead to different spin-orbit angles, and indeed systems with both small and large spin-orbit angles have been found (see, e.g., Winn et al. 2005; Hébrard et al. 2008; Johnson et al. 2009; Albrecht et al. 2012a; Brown et al. 2012). In addition Winn et al. (2010) and Albrecht et al. (2012b) presented evidence that all hot-Jupiter systems once had high obliquities, and that tides are responsible for the frequently observed low obliqui-

<sup>1</sup> Department of Physics, and Kavli Institute for Astrophysics and Space Research, Massachusetts Institute of Technology, Cambridge, MA 02139, USA

<sup>2</sup> Max-Planck-Institut für Astronomie, Königstuhl 17, 69117 Heidelberg, Germany

<sup>3</sup> Embassy of the Republic of Indonesia, Lehrter Str. 16-17, 10557 Berlin, Germany

<sup>4</sup> Harvard-Smithsonian Center for Astrophysics, Cambridge, MA 02138, USA

<sup>5</sup> Department of Astronomy and Astrophysics, University of California, Santa Cruz, Santa Cruz, CA 95064, USA

\* Based on observations made with ESOs 2.2m Telescopes at the La Silla Paranal Observatory under program ID 084.C-1008 (12.5%) and under MPIA guaranteed time (87.5%).

TABLE 1  
GENERAL DATA ON EP CRU

HD	109724	
NSV	5783	
R.A. <sub>J2000</sub>	12 <sup>h</sup> 37 <sup>m</sup> 17 <sup>s</sup>	†
Dec. <sub>J2000</sub>	−56°47′17″	†
Distance	1.0(1) kpc	*
V <sub>max</sub>	8.7 mag	*
Sp. Type	B5V+ B5V	*
Orbital period	11 <sup>d</sup> 08	*
Eccentricity	0.19	*
$R_p$	3.6(3) $R_\odot$	*
$R_s$	3.5(2) $R_\odot$	*
$M_p$	5(1) $M_\odot$	*
$M_s$	4.7(1.1) $M_\odot$	*
$T_{\text{eff}p}$	15 700(500)K	*
$T_{\text{eff}s}$	15 400(500)K	*

†Data from [ESA \(1997\)](#)

\*Data from [Clausen et al. \(2007\)](#)

NOTE. —  $R_p$  denotes the radius of the primary component and  $R_s$  the radius of the secondary component.  $M_p$  and  $M_s$  denote the masses  $T_{\text{eff}s}$  and  $T_{\text{eff}p}$  denote the effective temperatures.

ties. This suggests that the inward migration of hot Jupiters involves changes of the orbital planes of the planets.

With the BANANA project (Binaries Are Not Always Neatly Aligned) we aim to get a better understanding of the formation of close binaries as well as their tidal spin evolution. Here we study the EP Cru binary system. This is the fourth system which we study as part of the BANANA project ([Albrecht et al. 2007, 2009, 2011](#), Papers I–III). We also refer the reader to [Triaud et al. \(2013\)](#), for a description of a similar project by other investigators. While most of the stars in our sample are of early spectral types, their EBLM project focuses on eclipsing systems harboring low-mass stars.

EP Cru was only recently characterized by [Clausen et al. \(2007\)](#). Table 1 gives some system parameters. We selected this system because [Clausen et al. \(2007\)](#) found it to be similar to DI Her, for which we already found the spin-orbit angles to be very large ([Albrecht et al. 2009](#)). In particular the orbital parameters, the stellar masses, and the projected stellar rotation speeds ( $v \sin i_*$ ), are similar in these two systems. Here  $v$  indicates the equatorial rotation speed and  $i_*$  the inclination of the stellar rotation axis along the line of sight (LOS). There is one important difference between the two systems: the age of the stars. [Clausen et al. \(2007\)](#) estimated an age of  $\approx 50$  Myr for the two stars in the EP Cru system while DI Her is essentially a Zero Age Main Sequence (ZAMS) system with an estimated age of  $4.5 \pm 2.5$  Myr ([Claret et al. 2010](#)). Therefore by studying EP Cru we have the opportunity to learn if according to our current understanding of binary evolution one system is simply an older version of the other, or if they had different childhoods altogether.

The plan of this paper is as follows. In the following section we describe our observations. The analysis of the spectroscopic observations during eclipses and out of eclipses is presented in Section 3. We present the results on the absolute dimensions, the orientations of the stellar rotation axes, and the derived age in Section 4. For the remainder of the paper we focus on the interpretation of the obliquity measurements before we summarize our findings in the conclusions.

TABLE 2  
OBSERVATION LOG FOR EP CRU

Obs. Mid Time (BJD <sub>TDB</sub> )	Phase	Eclipse	S/N
2455192.85669	0.70	–	142
2455193.83164	0.78	–	97
2455194.69509	0.86	sec	77
2455194.83360	0.87	–	107
2455196.85095	0.06	–	107
2455197.86201	0.15	–	115
2455309.59755	0.24	pri	84
2455309.63874	0.24	pri	86
2455309.68141	0.24	pri	91
2455309.71894	0.25	pri	85
2455309.75526	0.25	pri	89
2455309.80483	0.25	pri	81
2455309.84282	0.26	–	71
2455309.86946	0.26	–	83
2455310.46906	0.31	–	73
2455311.46870	0.40	–	96
2455313.48255	0.59	–	94
2455314.57372	0.68	–	67
2455338.45972	0.84	sec	60
2455338.48823	0.84	sec	82
2455338.52361	0.85	sec	94
2455338.57536	0.85	sec	97
2455338.61565	0.85	sec	62
2455338.65529	0.86	sec	64
2455338.69515	0.86	sec	103
2455338.72942	0.86	sec	54
2455340.44257	0.02	–	78
2455341.55552	0.12	–	140
2455342.55950	0.21	pri	120
2455353.46096	0.19	–	130
2455353.50079	0.20	–	114
2455353.52531	0.20	–	144
2455353.57109	0.20	pri	123
2455353.61561	0.21	pri	137
2455353.65050	0.21	pri	128
2455360.46345	0.83	sec	83
2455360.53196	0.83	sec	89
2455360.60002	0.84	sec	53
2455360.64101	0.84	sec	44
2455361.49041	0.92	–	103
2455362.49566	0.01	–	88
2455628.85227	0.06	–	85
2455630.66346	0.22	pri	82
2455630.72346	0.22	pri	92
2455630.78472	0.23	pri	80
2455630.85156	0.24	pri	91
2455632.71659	0.40	–	83
2455635.68609	0.67	–	81

NOTE. — The phase is defined such that phase 0 corresponds to periastron. In column 3 ‘pri’ indicates that the observation was taken during a primary eclipse and ‘sec’ indicates that the observation was obtained during an ongoing secondary eclipse.

## 2. SPECTROSCOPIC OBSERVATIONS

We observed the EP Cru system with the FEROS spectrograph ([Kaufer et al. 1999](#)) on the 2.2 m telescope at ESO’s La Silla observatory. We obtained 48 observations on multiple nights between 2009 December and 2011 March. Table 2 gives an observation log. The observations had a typical integration time of 10 min. On each night, ThAr exposures

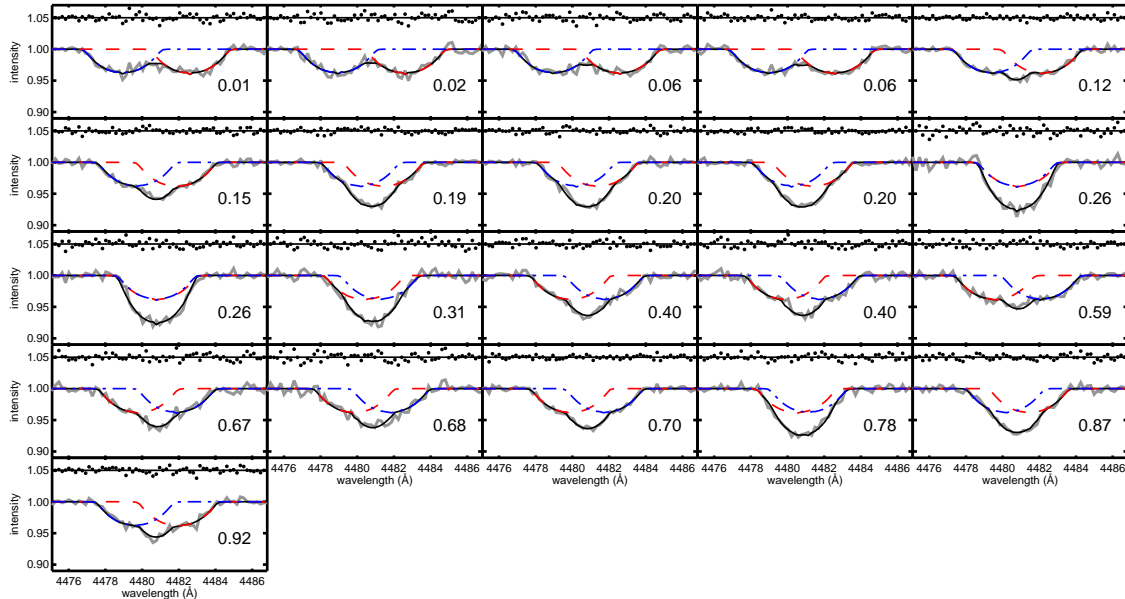


FIG. 1.— Spectra of EP Cru obtained at different orbital phases. Each panel shows spectra of both stars in the spectral region around the Mg II line. The orbital phase of the observation is indicated by the number in each panel, with phase 0 occurring at periastron passage. The gray solid lines represent the data and the (red) dashed and (blue) dash-dotted lines are the simulated absorption lines of the primary and secondary, respectively. The black line is the best fitting model. The dots around the line at a flux level of 1.05 represent the differences between the data and the model.

were taken to calculate a wavelength solution and monitor any changes in the spectrograph. For all observations we used the MIDAS FEROS package installed on the observatory computers to reduce the raw 2D CCD images and to obtain stellar flux as a function of wavelength. The uncertainty in the wavelength solution, expressed in velocity, is few  $\text{m s}^{-1}$ , and is negligible for our purposes. The resulting spectra have a resolution of  $\approx 50000$  around  $4481 \text{ \AA}$  (the wavelength area of the spectra we analyze). We corrected for the radial-velocity (RV) of the observatory, performed initial flat fielding with the nightly blaze function, and flagged and omitted bad pixels.

### 3. ANALYSIS

In this section we outline the analysis of the spectra with the aim of deriving absolute dimensions of the system and learning about the projected obliquities of both stars via measurements of the Rossiter-McLaughlin (RM) effect, which occurs during eclipses. We describe which part of spectrum we analyze and briefly introduce the model to which we compare the data and the algorithm used to extract system parameters. Our approach for EP Cru is similar to the approach employed in Papers I–III.

*Spectral region*— We focus on the Mg II line at  $4481 \text{ \AA}$ , as this line is relatively deep and chiefly broadened by stellar rotation. It is located in the red wing of the pressure-broadened He I line at  $4471 \text{ \AA}$ . While this line might also be included in the analysis (Albrecht et al. 2011), we decided here to exclude it as there is enough signal in the Mg II line and modeling the pressure broadening in the He I line represents an additional complication. Thus we fitted a Lorentzian model to the encroaching wing of the He I line and subtracted it before modeling the Mg II line. For this fit we used the spectral regions  $4472 - 4476 \text{ \AA}$  and  $4486 - 4498 \text{ \AA}$ , thereby avoiding the influence of the Mg II line. Each spectrum was binned to

a resolution of about  $12 \text{ km s}^{-1}$ , to speed up subsequent computations. Because the stellar rotation speeds are an order of magnitude larger, there is no significant loss of information due to the binning; we verified this by experimenting with higher resolutions.

*Model*— The measured spectra show absorption lines of both stars in the system. Before, during, and after eclipses the RVs of both stars are similar, leading to a substantial overlap of the two absorption lines. Hence, light emitted from both stars has to be accounted for when analyzing the RM effect. We used the numerical code from Albrecht et al. (2007) which simulates the spectra of both stars in a system.

The stellar disks are discretized with  $\sim 30,000$  pixels in a Cartesian coordinate system. We assume the stars to be spherical because they are well separated with rotation speeds much slower than the breakup velocity; Clausen et al. (2007) estimates an oblateness of about 0.0008. We further assume uniform rotation and quadratic limb darkening. Stellar surface velocity fields are parameterized adopting the macro-turbulence model by Gray (2005).<sup>7</sup> The coordinates of both stars projected on the sky are calculated and light from visible parts of the stellar hemispheres is integrated. The resulting absorption line kernels are shifted in wavelength corresponding to the line they represent and weighted according to the light contribution of the respective star.

*Parameter choices*— Having the model in place we can now learn about the EP Cru system by specifying a number of parameters. The Keplerian orbit of the two stars can be described with the following 6 parameters: The orbital period ( $P$ ), a specific time of minimum light during primary eclipse

<sup>7</sup> Here we do not need to take the point spread function (PSF) of the spectrograph into account as our binning ( $12 \text{ km s}^{-1}$ ) is larger than the width of the PSF ( $6 \text{ km s}^{-1}$ ).

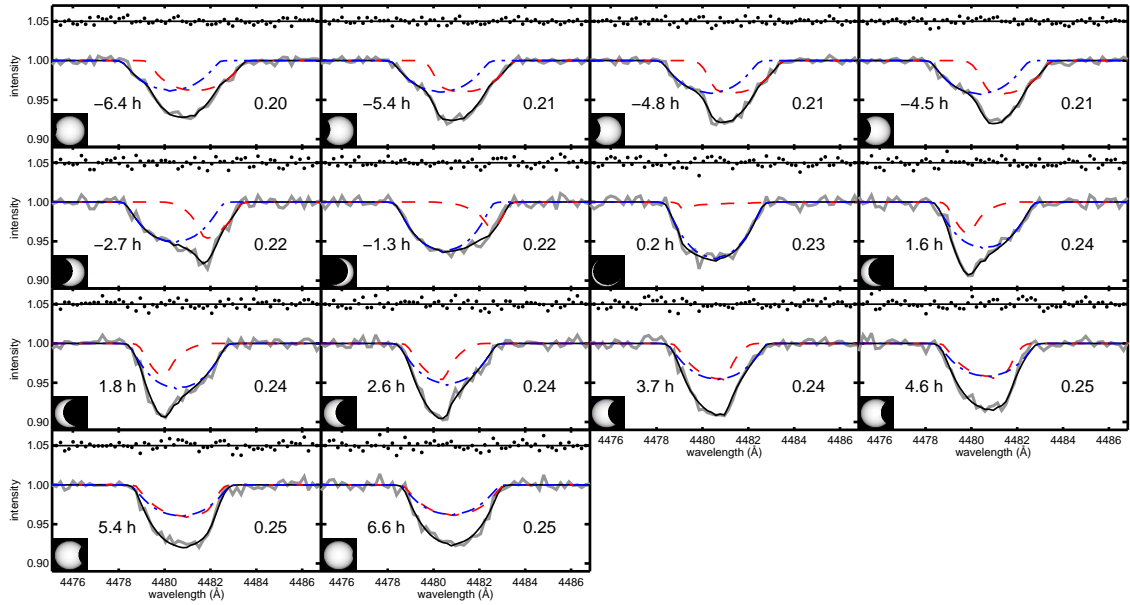


FIG. 2.— Spectra of EP Cru obtained during primary eclipse. Similar to Figure 1, but this time for observations obtained during primary eclipses. The numbers on the left side of each panel indicate the observation mid-exposure times relative to the time of minimum light, in hours. Each inset shows an illustration of the eclipse phase of the background star.

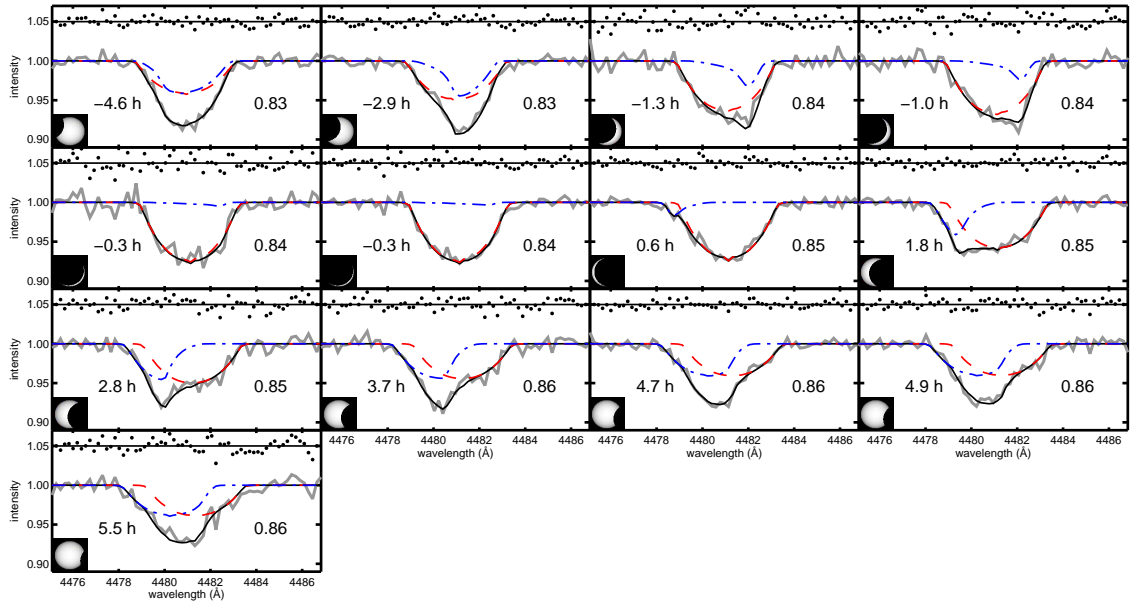


FIG. 3.— Spectra of EP Cru obtained during secondary eclipse. Similar to Figure 2, but for spectra obtained during secondary eclipses.

TABLE 3  
RESULTS FOR THE EP CRU SYSTEM.

Parameter	This Work	Literature Values
Orbital parameters		
Time of primary minimum, $T_{\min,1}$ (BJD-2 400 000)	46181.6928±0.0038	46181.7068±0.0003 <sup>1</sup>
Period, $P$ (days)	11.0774707±0.0000043	11.0774701±0.0000042 <sup>1c</sup>
$\sqrt{e} \cos \omega$	-0.104±0.006	
$\sqrt{e} \sin \omega$	0.4202±0.0011	
$e \cos \omega$	0.18187±0.00034	0.18162±0.00007 <sup>1</sup>
$e \sin \omega$	-0.0450±0.0026	-0.0475±0.0020 <sup>1</sup>
Eccentricity, $e$	0.1874±0.0005	0.1877±0.0005 <sup>1c</sup>
Argument of periastron, $\omega$ (deg)	346.1±0.7	345.4±0.6 <sup>1</sup>
Cosine orbital inclination, $\cos i_o$	0.0052±0.0014	
Orbital inclination, $i_o$ (deg)	89.70±0.08	86.97±0.09 <sup>1c</sup>
Velocity semi-amplitude primary, $K_p$ (km s <sup>-1</sup> )	102.2±1.5	100.9±1.3±10 <sup>1</sup>
Velocity semi-amplitude secondary, $K_s$ (km s <sup>-1</sup> )	106.2±1.4	105.9±3.5±10 <sup>1</sup>
Velocity offset, $\gamma_p$ (km s <sup>-1</sup> )	-26.3±0.6	-33 <sup>1</sup>
Velocity offset, $\gamma_p$ (km s <sup>-1</sup> )	-27.2±0.5	-33 <sup>1</sup>
Orbital semi-major axis, $a$ ( $R_\odot$ )	44.83±0.37	44.6±4.2 <sup>1</sup>
Stellar parameters		
Light ratio, $L_s/L_p$ @ 4480 Å	0.8972±0.0020	0.8972±0.0020 <sup>1c</sup>
Fractional radius primary, $r_p$	0.0801±0.0005	0.0810±0.0006 <sup>1c</sup>
Fractional radius secondary, $r_s$	0.0779±0.0004	0.0782±0.0006 <sup>1c</sup>
$u_1+u_2$	0.50±0.05	(0.4+0.1)±0.1 <sup>2c</sup>
Macro-turbulence parameter, $\zeta_p$ (km s <sup>-1</sup> )	22.3±1.7	
Projected rotation speed primary, $v \sin i_p$ (km s <sup>-1</sup> )	141.4±1.2±5	150 <sup>1</sup>
Projected rotation speed secondary, $v \sin i_s$ (km s <sup>-1</sup> )	137.8±1.1±5	150 <sup>1</sup>
Projected spin-orbit angle primary, $\beta_p$ (°)	-1.8±1.6	
Projected spin-orbit angle secondary, $\beta_s$ (°)	< 17 <sup>a</sup>	
Primary mass, $M_p$ ( $M_\odot$ )	5.02±0.13 <sup>b</sup>	4.95±1.06 <sup>1</sup>
Secondary mass, $M_s$ ( $M_\odot$ )	4.83±0.13 <sup>b</sup>	4.72±1.03 <sup>1</sup>
Primary radius, $R_p$ ( $R_\odot$ )	3.590±0.035 <sup>b</sup>	3.61±0.25 <sup>1</sup>
Secondary radius, $R_s$ ( $R_\odot$ )	3.495±0.034 <sup>b</sup>	3.48±0.24 <sup>1</sup>
Primary $\log g_p$ (cgs)	4.028±0.008	4.02±0.11 <sup>1</sup>
Secondary $\log g_s$ (cgs)	4.035±0.008	4.03±0.11 <sup>1</sup>

NOTES —

<sup>a</sup> We prefer this larger uncertainty interval over the statistical uncertainty of  $-13 \pm 4^\circ$  (Section 4.1).

<sup>b</sup> A solar radius of  $6.9566 \cdot 10^8$  m was used.

<sup>c</sup> Value was used as prior.

REFERENCES —

(1) [Clausen et al. \(2007\)](#) (2) [Claret \(2000\)](#)

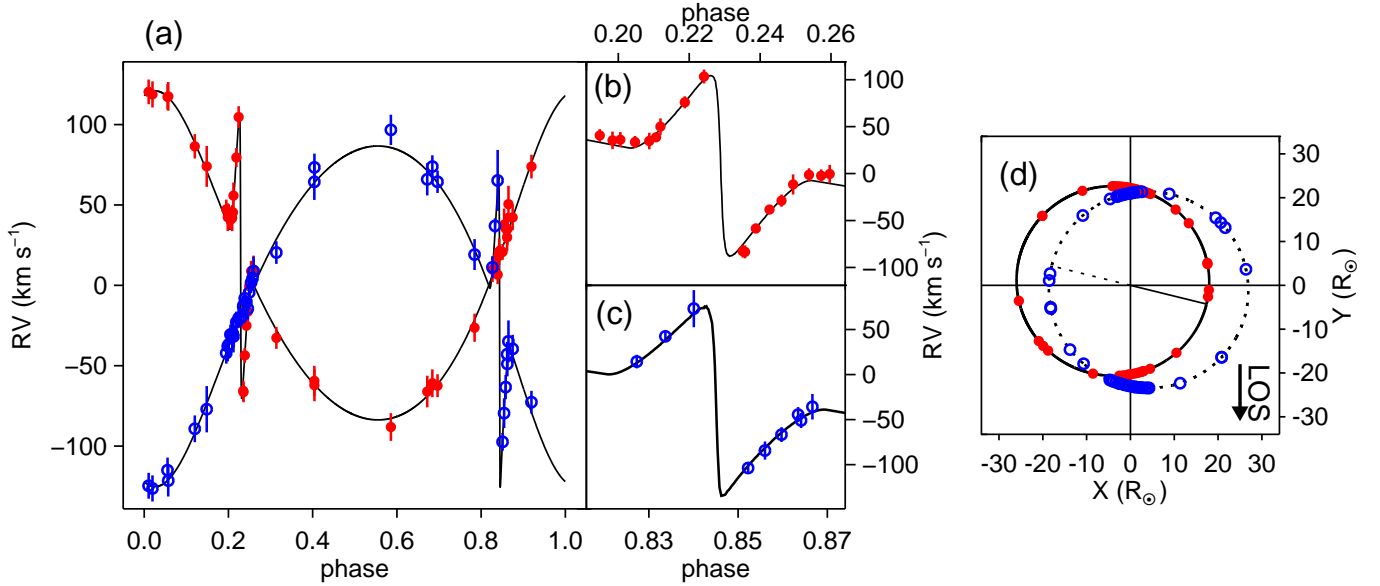


FIG. 4.— **Orbit of EP Cru.** (a) The apparent radial velocities (RV) in the EP Cru system for both stars as a function of orbital phase, defined such that phase zero occurs at periastron passage. The (red) filled circles indicate measured RVs of the primary and the open (blue) circles RVs of the secondary. Due to the small amount of light received from the eclipsed star during mid-eclipses it was not possible to assign RVs to the background stars for observations obtained within 1 hr of mid-eclipse. The RVs shown here were not used in the analysis; they are displayed only for illustrative purposes. (b) Zoom-in on orbital phases close to primary eclipse. Only RVs of the primary are shown. (c) The same as b, but this time for the secondary eclipse. (d) A pole on view of the orbit of both stars. The line of sight (LOS) towards earth is indicated.

( $T_{\min,1}$ ), the orbital eccentricity ( $e$ ), the argument of periastron ( $\omega$ ), and the velocity semi-amplitudes of the primary and secondary stars ( $K_i$ ). Here the subscript ‘i’ stands for either ‘p’ indicating the primary star or ‘s’ indicating the secondary (slightly less massive) star. In addition, velocity offsets ( $\gamma_i$ ) are needed. For  $e$  and  $\omega$  we use the stepping parameters  $\sqrt{e}\cos\omega$  and  $\sqrt{e}\sin\omega$ , as they are less correlated than  $e$  and  $\omega$  themselves. The results from the photometric study by Clausen et al. (2007) can be used to constrain some of these orbital parameters. However the photometry used by Clausen et al. (2007) was gathered about 20 years ago and the system is expected to have an apsidal motion period of a few thousand years. The change in  $\omega$  could be of order  $1^\circ$  over the last two decades. In addition the apsidal motion is not measured yet and we cannot calculate it from the known system parameters as it depends on the true stellar obliquity and not only the sky projection (Shakura 1985; Albrecht et al. 2009). Thus we do not use the photometric values on  $T_{\min,1}$  and  $\omega$  as priors and we only use the measurements of  $P$  and  $e$  by Clausen et al. (2007) as prior constraints. We revisit this subject in Section 4.3.

Additional parameters are needed to describe the projected equatorial rotation speeds ( $v\sin i_i$ ), the Gaussian width of the macro-turbulence ( $\zeta_i$ ), and the parameters of greatest interest for this study, the sky-projected spin-orbit angles ( $\beta_i$ ). The angle is defined according to the convention of Hosokawa (1953).

The photometric character of the eclipses are specified by another set of parameters: the light ratio between the two stars at the wavelength of interest ( $L_s/L_p$  at 4480 Å), the quadratic limb darkening parameters ( $u1_i$  and  $u2_i$ ), the fractional radii of the stars ( $r_i$ ), and the orbital inclination ( $i_o$ ), for which we step in  $\cos i_o$ . For the fractional radii and the orbital inclination we use prior information from Clausen et al. (2007). For  $L_s/L_p$  we use their results in the  $b$  band. To constrain the

limb darkening parameters we used the ‘jktld’<sup>8</sup> tool to query the ATLAS atmospheres (Claret 2000) and placed a Gaussian prior on  $u1_i + u2_i$  with a width of 0.1 and held the difference  $u1_i - u2_i$  fixed at the tabulated value.

An additional parameter is needed for each star to describe the relative depth of the Mg II lines. The Mg II line consists of a doublet, given the close spacing (0.2 Å) we model it here as single line.

The two components in the EP Cru system are very similar to each other (see Table 1). We therefore decided to use the same limb darkening parameters and macro-turbulence velocities, for both stars, thereby reducing the number of free parameters to 20. Of these, 7 are further constrained by Gaussian priors as explained above. Table 3 summarizes all of the prior constraints.

There is always a small residual uncertainty in the initial normalization of the spectra. To propagate this into the uncertainty intervals of the final parameters we added for each of the 48 observation 3 free parameters which describe a quadratic function used to normalize the continuum level. The values of the normalization parameters were optimized using a separate 3-parameter minimization for each observation, each time a set of system parameters is evaluated. This process is similar to the ‘‘Hyperplane Least Squares’’ method that was described and tested by Bakos et al. (2010).

*Parameter estimation* — A MCMC code was used to obtain uncertainty intervals. The chains consisted of 0.5 million calculations of  $\chi^2$ . The results reported below are the median values of the posterior distribution and the uncertainty intervals are the values which exclude 15.85 % of the values at each side of the posterior and encompassing 68.3 % of all values.

<sup>8</sup> <http://www.astro.keele.ac.uk/jkt/codes/jktld.html>

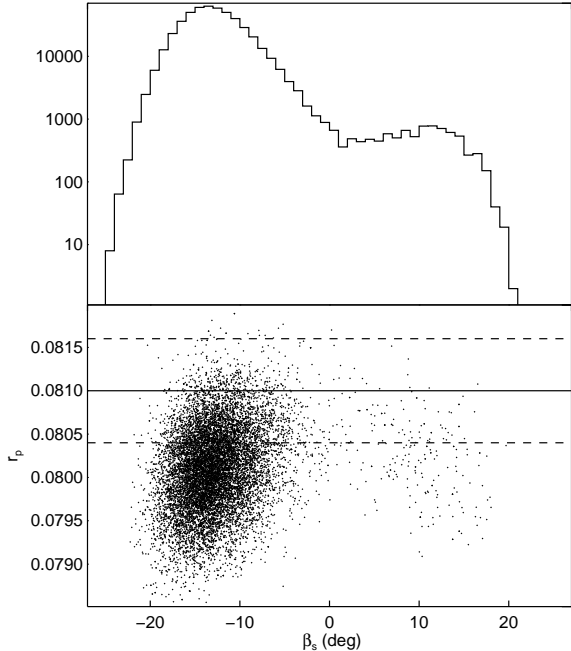


FIG. 5.— **Projected obliquity of the secondary star.** *Upper panel:* a histogram of the posterior of  $\beta_s$  with logarithmic y-axis. In addition to the main peak around an angle of  $-13^\circ$  there is a smaller peak at similar but positive values. *Lower panel:* a random sup-sample of the posterior in the  $\beta_s - r_p$  plane. The horizontal lines indicate the photometric prior and uncertainty interval for  $r_p$ . For larger values of  $r_p$  smaller absolute values of  $\beta_s$  are found.

#### 4. RESULTS

The results for the model parameters are given in Table 3. Figure 1 shows the spectra in the vicinity of the Mg II line and the corresponding model for the out-of-eclipse observations. Figures 2 and 3 show the same for the spectra obtained during primary and secondary eclipses. The apparent radial velocities in the EP Cru system are shown in Figure 4 as well as a pole-on view of the orbit.

##### 4.1. Stellar Rotation and Projected Obliquities

The main result of our analysis is that the sky projections of the two stellar rotation axes  $\beta_p = -1.8 \pm 1.6^\circ$  and  $\beta_s = -13 \pm 4^\circ$  indicate close alignment between the stellar rotation axes and the orbital angular momentum. However while the value for  $\beta_p$  is consistent with perfect alignment  $\beta_s$  seems to indicate a small but significant misalignment. How robust is this finding of a small misalignment? We note that we have somewhat lower S/N observations during the secondary eclipse than during the primary eclipse and fewer observations directly before, during and after the eclipse (See Table 2, and Figures 2, 3, and 4). To test the robustness of the result we reran the MCMC chain with different model assumptions. For example we constrained the model more, by leaving  $\gamma_i$  and the line depths of both stars tied to each other, or we left  $\zeta_i$  and the limb darkening parameters completely free. We also excluded some observations to test if a small number of observations are having a disproportionate influence on the result. For all these runs we found a negative  $\beta_s$ . The result closest to alignment was  $\beta_s = -9 \pm 5^\circ$ . At the same time the result for  $\beta_p$  did not change by more than  $0.4^\circ$  during these tests. There are, however, two peculiarities about our result for  $\beta_s$ . The posteriors for all the other parameters have only a single peak,

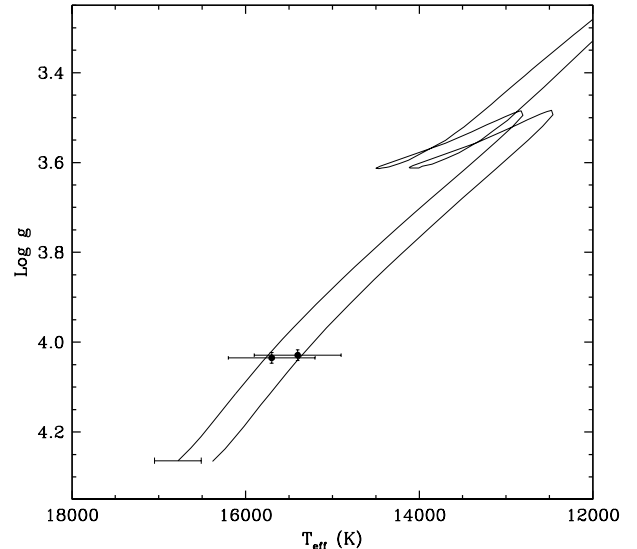


FIG. 6.— **Stellar evolution tracks for EP Cru** from the Yonsei-Yale series (Yi et al. 2001; Demarque et al. 2004) compared with the measurements. The tracks are interpolated to the measured masses and a metallicity of  $[\text{Fe}/\text{H}] = +0.03$  that best fits the temperatures. The uncertainty in the location of the tracks that comes from the mass error is indicated with an error bar for the primary, and is similar for the secondary. The age according to these models is  $57 \pm 5$  Myr.

while the posterior of  $\beta_s$  has a small (two orders of magnitude lower) secondary peak at positive angles around  $\beta_s = 13^\circ$  (Figure 5, upper panel). In addition there is a correlation between  $\beta_s$  and  $r_p$  (Figure 5, lower panel).  $r_p$  is the only parameter for which we do find a more than  $1-\sigma$  displacement between the prior constraints and results (Table 3). Taken the above mentioned points into consideration we are confident that  $|\beta_s| < 17^\circ$  but we cannot exclude a small projected obliquity for the secondary star, with the data at hand.

For the projected rotation speeds we find  $v \sin i_p = 141.4 \pm 1.2 \text{ km s}^{-1}$  and  $v \sin i_s = 137.8 \pm 1.1 \text{ km s}^{-1}$ . We consider the formal uncertainties in the  $v \sin i_i$  to be too low for the following reasons: We tested different limb darkening laws and found for example that for a linear limb darkening law the best fitting  $v \sin i$  values are lower by about  $4 \text{ km s}^{-1}$ . Also we suspect that our particular choice of parameterization of the stellar surface velocity fields will influence the values we find for the projected rotation. We therefore estimate that a uncertainty of  $5 \text{ km s}^{-1}$  is more realistic and also indicated that uncertainty in Table 3. As mentioned above, normalization for each observed spectrum is included in our routine, hence any uncertainty in normalization is already incorporated in the formal uncertainty.

We note that the projected rotation speeds are similar to the average rotation speed for B stars ( $v \sin i = 130 \text{ km s}^{-1}$ ), as analyzed by Abt et al. (2002). However the stars might have undergone a change of  $v$  due to tidal interactions (Section 5). Therefore we can not conclude from the similarity of the measured  $v \sin i$  to the expected  $v$  that  $\sin i$  is close to unity. Nevertheless it seems unlikely that the stars have large inclinations relative to the line of sight and at the same time their projected axes on the plane of the sky are both aligned. In what follows we assume that not only the projections of the rotation axes are small, but that the axes themselves are aligned too ( $\sin i \approx 1$ ).

Concerning the values for the macro-turbulence, we expect

TABLE 4  
EXPECTED APSIDAL MOTION IN EP CRU

Expected apsidal motion	(arcsec cycle <sup>-1</sup> )
$\dot{\omega}_{\text{GR}}$	$1.87 \pm 0.023$
$\dot{\omega}_{\text{Tides}}$	$0.76 \pm 0.11$
$\dot{\omega}_{\text{Rot}}$	$6.17 \pm 1.00$
$\dot{\omega}_{\text{Total}}$	$8.8 \pm 1.1$

NOTE. —  $\dot{\omega}_{\text{GR}}$  denotes apsidal motion due to General Relativity,  $\dot{\omega}_{\text{Tides}}$  due to tidal distortions, and  $\dot{\omega}_{\text{Rot}}$  due to rotational distortion.

that the value we find does not have a simple physical interpretation. This is because we assume equal brightness of raising and falling material as well as equal surface coverage of movement tangential and radial to the stellar surface, both assumptions do not need to be fulfilled in reality. We did test if there is a strong dependence of the measured values for projected obliquities on our adopted model for macro-turbulence, and found none.

#### 4.2. Absolute Dimensions and Age

From the posterior of our MCMC chain we find  $K_p = 102.2 \pm 1.5 \text{ km s}^{-1}$  and  $K_s = 106.2 \pm 1.4 \text{ km s}^{-1}$  in agreement with values from the literature (Table 3). We also calculated the  $K_i$  values only using out of eclipse data, making them less dependent on any assumption included in our eclipse model. With  $K_p = 101.9 \pm 1.5 \text{ km s}^{-1}$  and  $K_s = 106.2 \pm 1.6 \text{ km s}^{-1}$  we obtain consistent results.<sup>9</sup>

With the new spectroscopic data we not only obtain precise mass estimates for both stars but also improve on the absolute radii. This is because the accurate scaled radii  $r_i$  obtained via photometry need to be multiplied by the absolute scale of the system, the semi-major axis ( $a$ ).

With the new values for the stellar masses, surface gravities ( $\log g_i$ ), and the effective temperatures  $T_{\text{eff}i}$  measured by (Clausen et al. 2007, see also Table 1) we can estimate the stellar ages using stellar evolution models. Here we employ the Yonsei-Yale evolutionary tracks (Yi et al. 2001; Demarque et al. 2004). We find a good fit for solar metallicity and an age of  $57 \pm 5 \text{ Myr}$  (Figure 6). Another good check is the temperature difference between the stars, since the difference is probably better determined than the absolute temperatures. Indeed the temperature difference predicted by the models (i.e., the separation between the evolutionary tracks) is in good agreement with the temperature difference measured by Clausen et al. (2007).

#### 4.3. Apidal Motion

Now that the stellar rotation is known we can calculate the expected apsidal motion in the EP Cru system. We use the apsidal motion constant  $\log(k_2) = -2.3$  from Claret (2004) for both stars in the system. We assign an uncertainty of 0.1 in  $\log$  space to this constant. From the results in Table 4 we can see that we expect a shift of  $\approx 1.6 \pm 0.2^\circ$  over the last 20 years (which approximately have elapsed since the photometric measurements). Most of this shift is expected because of deformation of the stars by their rotation. That we

<sup>9</sup> John Southworth provided us with the 5 out of eclipse spectra used in the Clausen et al. (2007) study and we found that these are consistent with our data set. Because of the potential small change in the argument of periastron over the last 20 years they have not been included in this study.

TABLE 5  
EP CRU AND DI HER

Parameter	EP Cru	DI Her
Sp. Type	B5V+ B5V	B5V+ B5V*
$P$ (days)	11.08	10.55*
$e$	$0.1874 \pm 0.0005$	$0.489 \pm 0.003^*$
$M_p (M_\odot)$	$5.02 \pm 0.13$	$5.17 \pm 0.11^*$
$M_s (M_\odot)$	$4.83 \pm 0.13$	$4.52 \pm 0.07^*$
$R_p (R_\odot)$	$3.590 \pm 0.035$	$2.681 \pm 0.046^*$
$R_s (R_\odot)$	$3.495 \pm 0.034$	$2.478 \pm 0.046^*$
$\beta_p (^\circ)$	$-1.8 \pm 1.5$	$72 \pm 4^\dagger$
$\beta_s (^\circ)$	$< 17$	$-84 \pm 8^\dagger$
$v \sin i_p (\text{km s}^{-1})$	$141.4 \pm 5$	$108 \pm 4^\dagger$
$v \sin i_s (\text{km s}^{-1})$	$137.8 \pm 5$	$116 \pm 4^\dagger$
$v \text{syn}_p (\text{km s}^{-1})$	$16.40 \pm 0.16$	$12.85 \pm 0.24$
$v \text{syn}_s (\text{km s}^{-1})$	$16.04 \pm 0.15$	$11.89 \pm 0.24$
$v \text{ps}_p (\text{km s}^{-1})$	$19.51 \pm 0.19$	$34.3 \pm 0.7$
$v \text{ps}_s (\text{km s}^{-1})$	$19.00 \pm 0.18$	$31.8 \pm 0.7$
Age (Myr)	$57 \pm 5$	$4.5 \pm 2.5^\ddagger$

\*Data from Torres et al. (2010)

†Data from Albrecht et al. (2009)

‡Data from Claret et al. (2010)

NOTE. —  $v \text{syn}_i$  denotes the stellar rotation speed for an aligned star which rotation is synchronized with the orbital period.  $v \text{ps}_i$  denotes the pseudo synchronized value as defined by Hut (1981). To calculate  $v \text{ps}_i$  we used a  $\Omega_{\text{ps}}$  of 0.8 (see Hut 1981, Figure 3).

find a small increase in the argument of the periastron and a ( $\approx 22$  minutes) earlier primary eclipse than expected from linear ephemeris seems to indicate apsidal motion of the order of magnitude as expected. However spectroscopic data is not very good at determining  $\omega$  and we find it difficult to estimate the significance of the measured value for  $\omega$ . Therefore to make a meaningful comparison between the measured and expected apsidal motion, new photometric eclipse timings should be undertaken.

## 5. THE ALIGNMENT IN CONTEXT

Having established the absolute dimensions, age, and state of rotation in the EP Cru system we can now compare EP Cru to its apparently younger sibling DI Her. In Table 5 we reprint some of the values from EP Cru. According to these values the two systems are similar, apart from two characteristics: 1) their ages, EP Cru is about an order of magnitude older, 2) EP Cru appears to have aligned axes which is definitely not the case for DI Her. We would like to find a picture in which the misalignment in the young DI Her system can be explained as well as the alignment in the older EP Cru system.

Knowing that the scaled radii are large enough in these systems to allow for substantial tides, we might suspect that the difference in spin-orbit alignment is a result of observing these systems at different stages in their evolution rather than them having two different formation and evolution paths. The hypothesis would be that both stars had misaligned axes, and we see EP Cru with aligned axes only because it is older and tides have had enough time to align the axes.

The large eccentricities seen in both DI Her and EP Cru is consistent with this hypothesis, because tides first align and synchronize rotation and only on a longer timescale do they circularize the orbit. This is mainly due to the higher amount of angular momentum stored in the orbital motion compared



to the stellar rotation, and for systems with a low-mass secondary this is not necessary the case. However another finding makes the hypothesis difficult to reconcile with current tidal theories. The stars rotate at  $\sim 9$  times the speeds expected for synchronized or pseudosynchronized states (Table 5). Thus tides have not yet synchronized the stellar rotation speeds in the EP Cru system. Formulations of tidal interactions predict that damping of any significant spin-orbit misalignment should occur on the same time scale as synchronization of the rotation (Hut 1981; Eggleton & Kiseleva-Eggleton 2001).<sup>10</sup> This is because in these tidal models, a single coefficient describes the coupling between tides and rotation. When stellar rotation is much faster than the synchronized value rotation around any axis is damped by about the same amount. Thus the angle between the overall angular momentum and stellar spin does not change: only the rotation speed is reduced. When the stellar rotation around an axis parallel to the orbital angular momentum approaches the synchronized value than rotation around this axis couples less to tides. Rotation around any other axis is still damped by tides, which only ceases when the rotation around these axes stops. The stellar rotation aligns to the orbital axis.

To illustrate this point we used the TOPPLE tidal-evolution code developed by Eggleton & Kiseleva-Eggleton (2001). For this simulation we used the EP Cru parameters from Table 5 but with initial obliquities taken from DI Her, and an initial faster stellar rotation speed at zero-age main sequence. The results are shown in Figure 7. The stellar obliquities remain large until the stellar rotation speeds approach synchronization, at which point obliquities are damped. This suggests that EP Cru had aligned axes when it was as young as DI Her, implying in turn that DI Her and EP Cru do not represent different stages of one evolution, but rather two different evolution paths.

At the moment it is not possible to make more general statements as only a few measurements of obliquities have been carried out in close double-star systems. Furthermore most of these have been conducted in Algol systems which have undergone mass transfer (see Table 1 of Albrecht et al. 2011). Obliquity observations should be carried out in a variety of systems. Of particular interest would be young systems with short orbital periods with and without a third star. The systems should be young to minimize the influence of tides, they should have orbital periods ranging from few days to few tens of days. Obliquity measurements in these systems would be helpful in testing predictions of KCTF and thereby of close binary formation. Measurements of obliquities in wider systems would probe the length scale over which the primordial angular momentum was influential. Conducting such measurements is the aim of the BANANA project.

## 6. SUMMARY

We have analyzed high resolution spectra of the eclipsing close double star system EP Cru. We obtained absolute dimensions and showed that the rotation axes of both stars are aligned with each other and the orbital rotation ( $\beta_p = -1.8 \pm 1.6^\circ$  and  $|\beta_s| < 17^\circ$ ).

EP Cru is similar in its orbital and stellar characteristics to

DI Her. The two exceptions are that DI Her is younger and has

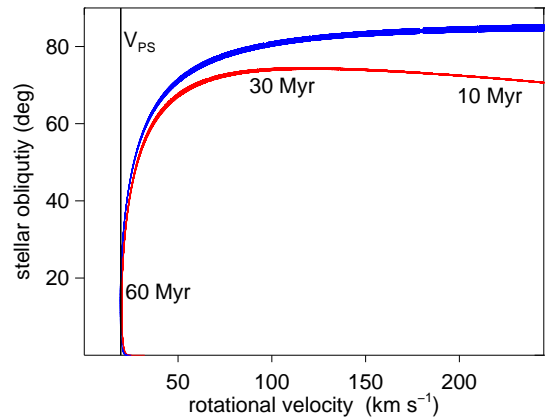


FIG. 7.— **Tidal evolution of a system similar to EP Cru, but with misaligned spin axes.** The blue and red lines show the evolutions of primary and secondary obliquities (angle between stellar spin and orbital plane) in a system with the parameters of EP Cru. However we started the run with obliquities which have been measured in the DI Her system and faster stellar rotation. We included the stellar evolution (in particular the change of the stellar radii with time) of the system as estimated with the  $Y^2$ -evolutionary tracks (Yi et al. 2001; Demarque et al. 2004) and set the viscous time ( $t_V$ ) to 50 000 years, about 1 000 times larger than what is normally assumed for late type stars. (A lower value of  $t_V$  would lead to an overall faster tidal evolution but will leave the ratio of the alignment and synchronization timescales unchanged.) There is little evolution in the stellar obliquities until the rotation speeds approach the pseudo-synchronized value for rotation ( $V_{PS}$ ), which is indicated by the vertical line and is currently similar for the two stars (Table 5).

two strongly misaligned stellar rotation axes. We have been unable to show that both systems represent different stages of one evolution path. This is because the stars in EP Cru rotate at a few times their synchronized value and tidal theory predicts that synchronization occurs around the same time as alignment. Therefore the two systems likely represent two different formation scenarios rather than two different evolutionary stages. The sample of close double star systems for which the obliquities are measured remains small. We plan to ratify this situation by measuring obliquities in more close double star systems in the framework of the BANANA project.

The authors are grateful to Peter Eggleton for insightful discussions on binary evolution and for making his TOPPLE code available to us. We thank John Southworth for providing us with the spectra used in the study by Clausen et al. (2007). S.A. acknowledges support during part of this project by a Rubicon fellowship from the Netherlands Organisation for Scientific Research (NWO). Work by S.A. and J.N.W. was supported by NASA Origins award NNX09AB33G and NSF grant No. 1108595. D.C.F. acknowledges NASA support through Hubble Fellowship grant HF-51272.01-A, awarded by STScI, operated by AURA under contract NAS 5-26555. This research has made use of the following web resources: [simbad.u-strasbg.fr](http://simbad.u-strasbg.fr), [adswww.harvard.edu](http://adswww.harvard.edu), [arxiv.org](http://arxiv.org), <http://arxiv.org>

<sup>10</sup> The timescales are not exactly equal, and which is faster depends on the ratio between the orbital and rotational angular momentum in the equilibrium states. For a system like EP Cru the timescale for pseudo synchronization is about twice the timescale for alignment (Hut 1981).

## REFERENCES

- Abt, H. A., Levato, H., & Grosso, M. 2002, *ApJ*, 573, 359
- Albrecht, S., Reffert, S., Snellen, I. A. G., & Winn, J. N. 2009, *Nature*, 461, 373
- Albrecht, S., Reffert, S., Snellen, I., Quirrenbach, A., & Mitchell, D. S. 2007, *A&A*, 474, 565
- Albrecht, S., Winn, J. N., Butler, R. P., et al. 2012a, *ApJ*, 744, 189
- Albrecht, S., Winn, J. N., Carter, J. A., Snellen, I. A. G., & de Mooij, E. J. W. 2011, *ApJ*, 726, 68
- Albrecht, S., Winn, J. N., Johnson, J. A., et al. 2012b, *ApJ*, 757, 18
- Bakos, G. Á., Torres, G., Pál, A., et al. 2010, *ApJ*, 710, 1724
- Bate, M. R., Lodato, G., & Pringle, J. E. 2010, *MNRAS*, 401, 1505
- Brown, D. J. A., Cameron, A. C., Anderson, D. R., et al. 2012, *MNRAS*, 423, 1503
- Claret, A. 2000, *A&A*, 363, 1081
- . 2004, *A&A*, 424, 919
- Claret, A., Torres, G., & Wolf, M. 2010, *A&A*, 515, A4
- Clausen, J. V., Helt, B. E., Giménez, A., et al. 2007, *A&A*, 461, 1065
- Demarque, P., Woo, J.-H., Kim, Y.-C., & Yi, S. K. 2004, *ApJS*, 155, 667
- Eggleton, P. P., & Kiseleva-Eggleton, L. 2001, *ApJ*, 562, 1012
- ESA. 1997, ESA SP-1200
- Fabrycky, D., & Tremaine, S. 2007, *ApJ*, 669, 1298
- Gray, D. F. 2005, *The Observation and Analysis of Stellar Photospheres*, 3<sup>rd</sup> Ed. (ISBN 0521851866, Cambridge University Press)
- Gualandris, A., Portegies Zwart, S., & Eggleton, P. P. 2004, *MNRAS*, 350, 615
- Hébrard, G., Bouchy, F., Pont, F., et al. 2008, *A&A*, 488, 763
- Hosokawa, Y. 1953, *PASJ*, 5, 88
- Hut, P. 1981, *A&A*, 99, 126
- Johnson, J. A., Winn, J. N., Albrecht, S., et al. 2009, *PASP*, 121, 1104
- Kafer, A., Stahl, O., Tubbesing, S., et al. 1999, *The Messenger*, 95, 8
- Kozai, Y. 1962, *AJ*, 67, 591
- Shakura, N. I. 1985, *Soviet Astronomy Letters*, 11, 224
- Thies, I., Kroupa, P., Goodwin, S. P., Stamatellos, D., & Whitworth, A. P. 2011, *MNRAS*, 417, 1817
- Tokovinin, A., Thomas, S., Sterzik, M., & Udry, S. 2006, *A&A*, 450, 681
- Torres, G., Andersen, J., & Giménez, A. 2010, *A&A Rev.*, 18, 67
- Triaud, A. H. M. J., Hebb, L., Anderson, D. R., et al. 2013, *A&A*, 549, A18
- Winn, J. N., Fabrycky, D., Albrecht, S., & Johnson, J. A. 2010, *ApJ*, 718, L145
- Winn, J. N., Noyes, R. W., Holman, M. J., et al. 2005, *ApJ*, 631, 1215
- Yi, S., Demarque, P., Kim, Y.-C., et al. 2001, *ApJS*, 136, 417
- Zahn, J.-P. 1977, *A&A*, 57, 383